IEEE Access
Multidisciplinary | Rapid Review | Open Access Journal

Received April 7, 2019, accepted May 9, 2019, date of publication May 14, 2019, date of current version May 28, 2019.

Digital Object Identifier 10.1109/ACCESS.2019.2916899

Detecting Positive and Negative Changes From SAR Images by an Evolutionary Multi-Objective Approach

SHUANG LIANG[1], HAO LI[1], YUN ZHU[2], AND MAOGUO GONG[1], (Senior Member, IEEE)

[1]School of Electronic Engineering, Key Laboratory of Intelligent Perception and Image Understanding, Ministry of Education, Xidian University, Xi'an 710071, China

[2]School of Computer Science, Key Laboratory of Modern Teaching Technology, Ministry of Education, Shaanxi Normal University, Xi'an 710119, China

Corresponding author: Hao Li (omegalihao@gmail.com)

This work was supported in part by the National Natural Science Foundation of China under Grant 61772393, in part by the National Key Research and Development Program of China under Grant 2017YFB0802200, and in part by the Key Research and Development Program of Shaanxi Province under Grant 2018ZDXM-GY-045.

ABSTRACT In general, changes in the multitemporal synthetic aperture radar (SAR) images are detected by classifying the SAR ratio images into the changed and unchanged classes. However, multitemporal SAR images have either increase or decrease in the backscattering values. Therefore, the changed areas can be further classified into positive and negative changed classes. This paper presents an unsupervised change detection approach for detecting the positive and negative changes based on a multi-objective evolutionary algorithm. In this paper, the widely adopted mean-ratio and log-ratio operators are extended to generate SAR ratio images for distinguishing the positive and negative changes. In order to reduce the corruption of speckle noise present in the multitemporal SAR images, a fuzzy cluster validity index is established to exploit local spatial and gray level information. Then the objective functions are simultaneously optimized by a multi-objective evolutionary algorithm. The experimental results on two simulated data sets and three real SAR data sets confirm the effectiveness of the proposed method.

INDEX TERMS Evolutionary algorithm, image change detection, multi-objective optimization, synthetic aperture radar.

I. INTRODUCTION

Image change detection is a process that detects the changes between two multitemporal images of the same scene. By the end of the last decades, change detection in remote sensing images [1]–[6] has become increasingly important in the field of satellite image processing with the development of remote sensing technology. Synthetic aperture radar (SAR) images [7]–[18] have become valuable sources of information in change detection because SAR systems can keep working in various weather conditions and are not affected by cloud cover or different sunlight conditions, which can make up the shortage of optics and infrared remote sensing. Generally speaking, the process of change detection in SAR images includes the following two steps. First, an intermediate image is generated from two multitemporal SAR images. The ratio operator is a well-known technique used in the process of image change detection. Second, in most literatures, the intermediate image is segmented into the unchanged and changed classes as the problem is usually viewed as a binary classification problem.

Due to the fact that SAR images suffer from speckle noise, it is rather difficult to do such segmentation. The source of speckle noise can be attributed to random interference between the coherent returns issued from the numerous scatterers present on a surface. Speckle noise manifests itself in the form of a random pixel-to-pixel variation with statistical properties similar to those of thermal noise and makes it difficult to visually and automatically interpret SAR data [19]. To overcome the defect inherently characterizing SAR images, in many literatures, researchers have tried to utilize different algorithms to reduce the corruption of the speckle noise. In the first step, the mean-ratio (MR) operator [10] and log-ratio (LR) operator [13] are well-known techniques for producing SAR ratio image because of the multiplicative nature of speckle. In the second step, the ratio image can be

The associate editor coordinating the review of this manuscript and approving it for publication was Ran Cheng.

analyzed by using image segmentation methods. One of the popular methods to identify the changes is the thresholding approach, such as Ostu, the Kittler and Illingworth minimum error thresholding algorithm, and the expectation maximization (EM) algorithm. They are carried out by applying a thresholding procedure to the histogram of the SAR ratio image. The decision of an accurate model to fit the two classes is important. Bazi *et al.* [14] used the Generalized Gaussian distribution to model the changed and unchanged classes. And many probability density function such as Log normal, Generalized Gaussian, Nakagami ratio, and Weibull ratio were investigated to model the distribution of the two classes in [15]. In [16], Hu and Ban proposed an automatic and effective approach to the thresholding of the log-ratio operator whose histogram may be multimodal. Furthermore, the clustering approaches are also widely used in change detection, which do not involve such a process to build a model. In order to be robust to noise, many algorithms incorporating local information were proposed in recent years [17], [20], [21]. In [21], Gong *et al.* proposed a reformulated fuzzy local-information C-means (RFLICM) for classifying changed and unchanged areas, which incorporates the information about spatial context by adding a new fuzzy factor into its objective function for the purpose of enhancing the changed information and reducing the effect of speckle noise. In [12], [17], Markov random field (MRF) based change detection algorithms were proposed to combat speckle noise, which provides a basis for modeling information about the mutual influences among image pixels. And non-local means (NLM) that utilizes nonlocal relationship between image pixels were also used in many change detection techniques [9], [12].

In some cases, the multitemporal SAR images have either increase or decrease in the backscattering values. Therefore SAR image change detection is expected to be developed for three-class classification problems, i.e., the changed class is further classified into the positive and negative changed classes. In the thresholding based change detection methods, changes are assumed to be on one side of the histogram of the SAR ratio image, which is not true for all change detection problem [18]. In particular, changes may be present on both sides of the histogram of the SAR ratio image and two decision thresholds should be used to detect the changes. In the clustering based change detection methods for three classes, the initial number of the cluster centers should be set three to classify the SAR ratio images into three classes.

For detecting positive and negative changes, no single validity measure works well on different kinds of SAR data sets [9], [12], [21], and what's worse, it makes the change detection problem complicated to subdivide the changed areas. In this paper, we adopt an evolutionary multi-objective approach and show how it can be successfully used to detect the positive and negative changes. Multi-objective evolutionary algorithms (MOEAs) can optimize several conflicting objectives simultaneously and are able to generate a set of non-dominated solutions in a single run [22], [23]. MOEAs have been successfully applied in many applications, such as data clustering [24]. MOEA-based clustering algorithms have found many applications for segmentation of color images, MRI medical imagery [25], [26] and remote sensing imagery [27], [28]. Handl and Knowles proposed a multi-objective clustering technique with automatic k-determination (MOCK) [29], and it considers a clustering task as a multi-objective optimization problem solving data clustering problems unconventionally and shows good performance. Bandyopadhyay *et al.* [27] used the Xie-Beni (XB) index [30] and the fuzzy C-means (FCM) measure [31] as the objective functions for pixel classification in remote sensing images. There are also several multi-objective methods which use more than two objective functions. Three validity indices, viz., XB index, the FCM measure and PBM index have been optimized simultaneously in [26]. Furthermore, several MOEAs have been used as the fundamental optimization tool for multi-objective clustering. The MOCK algorithm used pareto envelope-based selection algorithm-II (PESA-II) [32] for the clustering problem. Non-dominated sorting genetic algorithm-II (NSGA-II) [33] has been employed in [25], [28], [34] as the underlying optimization tool.

In this paper, a novel change detection technique is proposed to detect the positive and negative changes in multitemporal SAR images. In the proposed method, the MR operator and the LR operator are modified to contain the positive and negative change information. Due to the presence of the speckle noise, single validity measure does not work well to detect the positive and negative changes. Therefore, in this paper, a multi-objective evolutionary algorithm based on local information is proposed to optimize multiple validity measures simultaneously. The FCM measure, the XB index and the FCM based local term are used as the objective functions. Finally, the proposed method is able to obtain a set of nondominated solutions for representing the trade-off among these objectives.

The rest of this paper is organized as follows: The background knowledge is described in Section II. Section III introduces the generation of ratio images and the proposed multiobjective clustering method in detail. Experimental settings are shown in Section IV and experimental results are described in Section V. Finally, concluding remarks are given in Section VI.

II. BACKGROUND

Without loss of generality, the multi-objective optimization problems (MOPs) in this paper can be set for minimization. An MOP can be stated as

$$\begin{aligned} &\min \ F(x) = (f_1(x), \cdots, f_m(x))^T \\ &\text{subject to } \ x \in \Omega \end{aligned} \tag{1}$$

where Ω is the feasible space, x is a solution to the MOP, R^m is the objective space, and the $F : \Omega \rightarrow R^m$ consists of m real-valued objective functions. In most instances, the objectives in an MOP are contradictory to each other, which means no

point in feasible space can minimize all the objectives simultaneously. Hence, multi-objective optimization [22], [35] are designed to find the best trad-off relationship among them simultaneously.

For minimization, a solution x_u is said to dominate another solution x_v, if and only if

$$\begin{aligned} &\forall i = 1, 2, \cdots, m\, f_i(x_u) \leq f_i(x_v) \\ &\exists j = 1, 2, \cdots, m\, f_i(x_u) < f_i(x_v) \end{aligned} \tag{2}$$

And a point x^* in Ω is called a Pareto optimal solution to (1) on condition that there is no such point x in Ω that makes $F(x)$ dominate $F(x^*)$. Then $F(x^*)$ is termed as Pareto optimal vector. The objectives in a Pareto optimal vector have such relationship: a decrease in one objective causes an increase in the others. All the Pareto optimal points constitute a set called Pareto optimal set [36], and their corresponding Pareto optimal objective vectors are called the Pareto optimal front (PF) [36].

For multi-objective optimization, it has been recognized that evolutionary algorithms (EAs) are well suited because EAs can deal with a set of possible solutions simultaneously [23], [35]. Since [37], various EAs to deal with MOPs have been proposed such as [33], [38]–[41] and these EAs are termed as multi-objective evolutionary algorithms (MOEAs). MOEAs seek to obtain a set of Pareto optimal solutions for approximating the true PF in a single run. For change detection in SAR images, the techniques that optimize a single objective may not provide satisfactory result on different data sets. MOEAs can simultaneously optimize several objectives and user usually can choose a suitable one from the final change detection results.

III. METHODOLOGY

In this section, the proposed change detection algorithm for detection the positive and negative changes is described. First, the generation of the ratio images is stated. Next, the choice of objective functions is given. Then the formulas for updating the membership values are shown. Finally, an evolutionary algorithm is used to search the optimal cluster centers.

The proposed algorithm for SAR image change detection is described in **Algorithm 1**. In the proposed change detection framework, three conflicting objective functions are optimized by MOEAs simultaneously which builds a population of competing individuals and ranks them on the basis of nondominance. A real-coded crossover and mutation operator are used in the proposed method. The nondominated solutions among the parent and child population are propagated to the next generation. The better individuals remain unknown until all candidates are sorted and assigned a crowding distance and non-domination level. Parents are selected for mating using a tournament selection operator which uses the rank and crowding distance of individuals. The offsprings are generated from the selected parents. Then the offsprings are evaluated on the objective functions. Following this, they are combined with the parent generation. The combined population is then sorted into dominance ranks.

Algorithm 1 Algorithm of Detecting Positive and Negative Changes

Input: N_p: population size, *maxgen*: max generation number.
Output: Change detection maps.

1 Step 1) Generate the SAR ratio image I_R by Eq. (6) or Eq. (8) described in Section II.
2 Step 2) Initialization: Set $t = 0$, generate the initial population P^0 with size N_p.
3 Step 3) Cycling
4 Step 3.1) Create a new population of offspring with the implementation of crossover, mutation, and selection operators.
5 Step 3.2) Combine the parents and offspring to create the next population.
6 Step 4) If $t < maxgen$ then $t = t + 1$ and go to Step 3) for the next cycle, otherwise, stop the algorithm and go to next step.
7 Step 5) Obtain the membership partition matrix with the best cluster centers. The change detection maps are generated according to the membership partition matrix.

A. GENERATING THE RATIO IMAGES FOR DETECTING POSITIVE AND NEGATIVE CHANGES

Let us consider two coregistered SAR images, $I_A = \{I_A(i,j), 1 \leq i \leq H, \ 1 \leq j \leq W\}$ and $I_B = \{I_B(i,j), \ 1 \leq i \leq H, \ 1 \leq j \leq W\}$ of size $H \times W$. Both of them are acquired over the same geographical area at two different times t_1 and t_2, respectively. For a SAR image, the image intensity I is related to the underlying backscattering coefficient X by the multiplicative model

$$I = FX \tag{3}$$

where F is the normalized fading speckle-noise random variable.

SAR ratio images are obtained by applying a pixel-by-pixel ratio operator to the considered multitemporal SAR images. However, for change detection in SAR images, it is difficult to undertake a precise detection due to the existence of speckle, and some unchanged areas may falsely detected, whereas some changed areas may be undetected [42]. Since the ratio method is sensitive to speckle noise, the ratio images are usually shown in a mean or a logarithmic scale. The mean-ratio image I_{MR} is commonly given by [10]

$$I_{MR} = 1 - \min\left(\frac{\mu_A}{\mu_B}, \frac{\mu_B}{\mu_A}\right) \tag{4}$$

where μ_A and μ_B represent the local mean values of multitemporal SAR images I_A and I_B, respectively.

Furthermore, the log-ratio method is also robust to speckle noise. With the LR operator, the multiplicative speckle noise can be transformed in an additive noise component and the range of variation of the ratio image will be compressed and thereby enhances the low-intensity pixels. The information

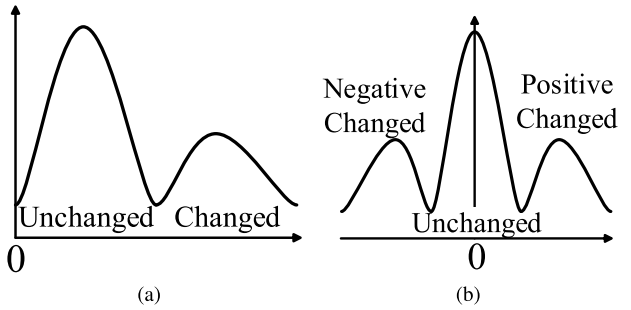

FIGURE 1. Schematic plots for change detection.

of background is relatively flat on account of the logarithmic transformation. The log-ratio image I_{LR} is widely used by many researchers, which is commonly given as

$$I_{LR} = \left|\log \frac{I_B}{I_A}\right| = \left|\log \frac{F_B}{F_A} + \log \frac{X_B}{X_A}\right| \tag{5}$$

As shown in Fig. 1(a), in the two-class SAR image change detection, the unchanged pixels show small values and changed pixels show larger values by using the MR operator in Eq. (4) and the LR operator in Eq. (5). However, Eq. (4) and Eq. (5) do not consider the positive and negative changes of the considered multitemporal SAR images. As shown in Fig. 1(b), we expect that the positive changed pixels present large positive values and the negative changed pixels present negative values with large absolute values. Therefore, the unchanged pixels exhibit smaller absolute values. We need to modify Eq. (4) and Eq. (5) to generate ratio images, which can represent the positive and negative change information. In the MR operator, the values of μ_A and μ_B should be compared to distinguish the positive and negative changes. The above formula in Eq. (4) can be rewritten as

$$I_{MR} = \begin{cases} 1 - \min\left(\dfrac{\mu_A}{\mu_B}, \dfrac{\mu_B}{\mu_A}\right), & \text{if } \mu_B > \mu_A \\ -\left[1 - \min\left(\dfrac{\mu_A}{\mu_B}, \dfrac{\mu_B}{\mu_A}\right)\right], & \text{if } \mu_A \geq \mu_B \end{cases} \tag{6}$$

By comparing μ_A and μ_B, changed pixels are classified into the positive and negative changed classes. If μ_A are larger than μ_B, the pixels in the mean-ratio image exhibit negative values. Therefore Eq. (6) is able to express the positive and negative changes of the multitemporal images. The same method is used to modify the log-ratio operator. The formula for generating log-ratio images is shown as

$$I_{LR} = \begin{cases} \log I_B - \log I_A, & \text{if } I_B > I_A \\ -(\log I_A - \log I_B), & \text{if } I_A \geq I_B \end{cases} \tag{7}$$

and Eq. (7) can be rewritten as

$$I_{LR} = \log \frac{I_B}{I_A} \tag{8}$$

Obviously, it is easy to get the log-ratio images for containing the positive and negative change information by removing the absolute value symbol of the above formula in Eq. (5). If I_B is smaller than I_A, the pixels in the log-ratio images exhibit negative values, which represent negative changes. The process of generation of SAR ratio images for change detection has the following steps: 1) Image preprocessing is implemented to obtain the SAR images I_A and I_B, which mainly includes coregistration, geometric corrections, and noise reduction. 2) Generate the initiatory SAR ratio images I_{MR} or I_{LR} using the mean-operator in Eq. (6) or the log-ratio operator in Eq. (8), respectively.

B. SELECTING THE OBJECTIVE FUNCTIONS

The choice of objective functions should be as contradictory as possible, which has an important impact on the performance of the proposed method. In the multi-objective fuzzy clustering framework, two conflicting and complementary indices, called J_m and XB, are used as two optimization objectives. J_m is the energy function of the standard FCM algorithm, which is one of the most popular clustering methods for image segmentation. The energy function J_m of the standard FCM algorithm for partitioning a data set $\{x_i\}_{i=1}^N$ into c clusters is described as

$$J_m = \sum_{i=1}^{N}\sum_{k=1}^{K} u_{k,i}^m D^2(z_k, x_i) \tag{9}$$

where m is a weighting exponent on each fuzzy membership, N is the number of pixels in the image, K is the number of clusters with $2 \leq K \leq N$ (K is equal to 3 in this paper), x_i is the ith pixel in the image, $u_{k,i}$ is the degree of membership of x_i in the kth cluster, and $D^2(z_k, x_i) = \|x_i - z_k\|^2$ denotes the distance of point x_i from the centre of the kth cluster.

The XB index is defined as a function of the ratio of the total variation σ to the minimum separation sep of the clusters. Here σ and sep are shown as

$$\sigma(u, z, x) = \sum_{k=1}^{K}\sum_{i=1}^{N} u_{k,i}^m D^2(z_k, x_i) \tag{10}$$

and

$$sep(z) = \min_{i \neq j} \|z_k - z_j\|^2 \tag{11}$$

where $\|\cdot\|$ denotes the Euclidean norm. The XB index is then defined as

$$XB = \frac{\sigma(u, z, x)}{N \times sep(z)} \tag{12}$$

Note that when the partitioning is compact and the individual clusters are well separated, value of σ should be low while sep should be high, thereby yielding lower values of XB index.

As mentioned above, it is a hard work to keep trade-off between robustness to noise and effectiveness of preserving the details. Hence, a local information index [20] (called LI) is employed to reduce the effect of speckle noise.

$$LI = \sum_{i=1}^{N}\sum_{k=1}^{K}\sum_{j \in N_i, j \neq i} \frac{1}{d_{ij} + 1}(1 - u_{kj})^m \left\|x_j - v_k\right\|^2 \tag{13}$$

0.414	0.5	0.414
0.5		0.5
0.414	0.5	0.414

(a)

0.261	0.309	0.333	0.309	0.261
0.309	0.414	0.5	0.414	0.309
0.333	0.5		0.5	0.333
0.309	0.414	0.5	0.414	0.309
0.261	0.309	0.333	0.309	0.261

(b)

FIGURE 2. Damping extent of the neighboring pixels. (a) 3 × 3; (b) 5 × 5.

where the ith pixel is the center of the local window, the jth pixel belongs in the set of the neighbors falling into a window around the ith pixel (N_i). $d_{i,j}$ is the spatial Euclidean distance between pixel i and j. The damping extent [20] of the neighboring pixels with the size of 3 × 3 and 5 × 5 are shown in Fig. 2.

The *LI* index controls the influence of the neighborhood pixels depending on their distance from the central pixel by incorporating both local spatial and gray level relationship. The local gray level relationship not only varies automatically according to different gray level difference between the pixels over an image, but also is dependent on their fuzzy membership values. The *LI* index is used here as the third objective function to restrain noise in the SAR ratio images.

C. UPDATING THE MEMBERSHIP VALUES

For computing the above objective functions, the cluster centers encoded in a chromosome are first obtained by evolutionary algorithm. In the original multi-objective genetic fuzzy clustering algorithm, the membership values are computed as [27]

$$u_{ki} = \frac{1}{\sum_{j=1}^{c} \left(\frac{\|x_i - z_k\|^2}{\|x_i - z_j\|^2} \right)^{\frac{1}{m-1}}} \tag{14}$$

However, due to the incorporation of the *LI* index, the calculation of the membership partition matrix and the cluster centers is performed as [20]

$$u_{ki} = \frac{1}{\sum_{j=1}^{K} \left(\frac{\|x_i - v_k\|^2 + G_{ki}}{\|x_i - v_j\|^2 + G_{ji}} \right)^{\frac{1}{m-1}}} \tag{15}$$

where

$$G_{ki} = \sum_{j \in N_i, j \neq i} \frac{1}{d_{ij} + 1} (1 - u_{kj})^m \left\| x_j - v_k \right\|^2 \tag{16}$$

D. UPDATING THE CLUSTER CENTERS BY EVOLUTIONARY ALGORITHM

Real-valued chromosomes representing the coordinates of the centers of the three classes are used. And a hybrid initialization method based on thresholding is used to generate the initial populations. A 80% probability of the centers encoded in the chromosomes are randomly selected. A 20% probability of the centers are generated by a thresholding-based initialization method. In the three-class image change detection, two decision thresholds T_1 and T_2 are obtained by the GGKI algorithm proposed in [18]. Then the values of the centers are generate between $[0, T_1]$, $[T_1, T_2]$, and $[T_2, L-1]$, respectively.

Conventional single-point crossover operation, applied stochastically with crossover probability p_c, has been performed to generate the new offspring solution from the chromosomes selected in the mating pool. For performing the mutation, a mutation probability p_m has been used. If a chromosome is selected to be mutated, the gene position that will undergo mutation is selected randomly. The polynomial mutation used in NSGA-II is chosen as the mutation operator. In order to generate the mating pool of chromosomes, crowded binary tournament selection [43] in NSGA-II is utilized here. After selection, the selected chromosomes are put in the mating pool.

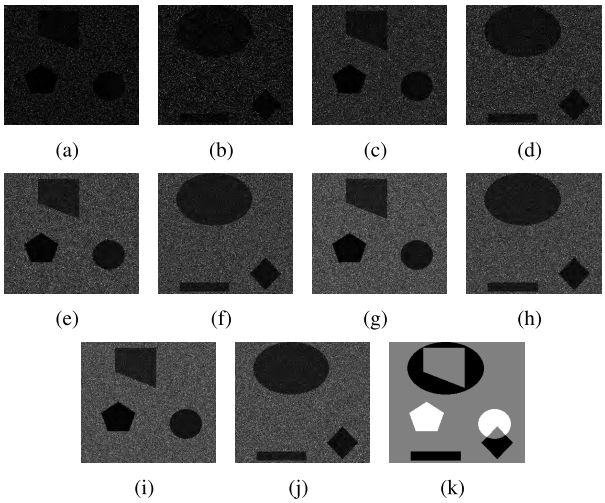

FIGURE 3. A simulated data set with five pairs of SAR images with different ENLs (Simulated data set I). (a) and (b): ENL = 1. (c) and (d): ENL = 2. (e) and (f): ENL = 3. (g) and (h): ENL = 4. (i) and (j): ENL = 5. (k) The reference image.

IV. EXPERIMENTAL SETTINGS

In this section, two simulated data sets and three SAR images data sets considered in our experiments are introduced. Then some evaluation criteria for change detection and parameter settings for our experiments are described in detail. In the change detection maps, the positive and negative changed pixels are labeled with white and black color, respectively. And the unchanged pixels are labeled with gray color.

A. DATA SETS

The first data set is a simulated data set. Equal number of looks (ENL) indicates the noise level of SAR images and lower value of ENL indicates higher noise level. This data set has five pairs of simulated SAR images with ENL = 1, 2, 3, 4, and 5, respectively. As shown in Fig. 3,

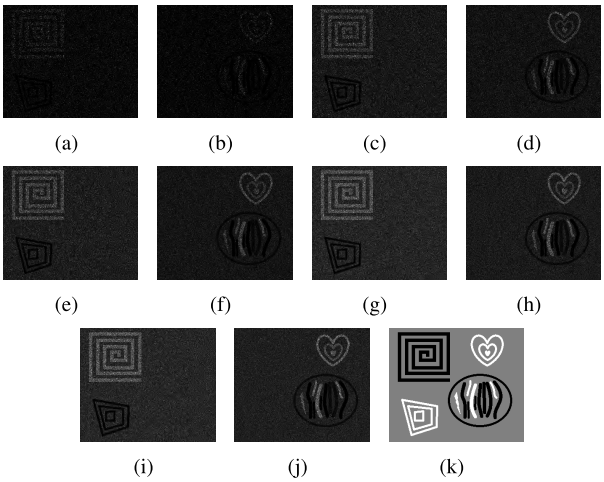

FIGURE 4. A simulated data set with five pairs of SAR images with different ENLs (Simulated data set II). (a) and (b): ENL = 1. (c) and (d): ENL = 2. (e) and (f): ENL = 3. (g) and (h): ENL = 4. (i) and (j): ENL = 5. (k) The reference image.

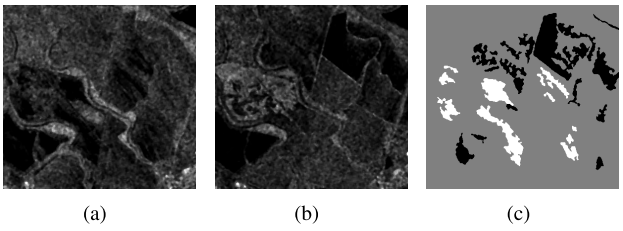

FIGURE 5. San Francisco data set. (a) The image acquired in August 2003. (b) The image acquired in May 2004. (c) The ground truth image.

six geometric figures are shown in these images with different relations, such as appearing, disappearing and overlapping. The reference image with three classes is shown in Fig. 3(k).

The second data set is also a simulated data set. This data set has five pairs of simulated SAR images with ENL = 1, 2, 3, 4, and 5, respectively. As shown in Fig. 4, these images have different textures. The reference image with three classes is shown in Fig. 4(k). The first and second data sets with different characteristics are used here to analyze the influence of noise level on the change detection results.

The third data set (7713 × 7749) contains a set of SAR images collected on the city of San Francisco, California. This data set was acquired by the ESA ERS-2 satellite on August 10, 2003 and May 16, 2004. One area of size 390 × 370 is selected as a representative test site. The available ground truth is generated by integrating prior information. The images with photo interpretation are shown in Fig. 5.

The fourth and fifth data sets used in the experiments considered of two SAR images acquired by Radarsat-2 at the area of Yellow River Estuary in China in June 2008 and June 2009, respectively. The fourth data set (260 × 290) with photo interpretation is shown in Fig. 6. There is no ground truth image provided for the fifth data set (565 × 510), which is shown in Fig. 7.

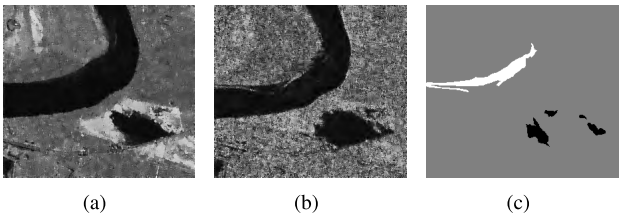

FIGURE 6. One area of Yellow River Estuary data set (Yellow River data set I). (a) The image acquired in June 2008. (b) The image acquired in June 2009. (c) The ground truth image.

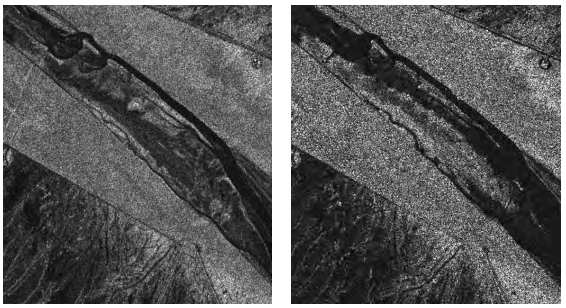

FIGURE 7. One area of Yellow River Estuary data set (Yellow River data set II). (a) The image acquired in June 2008. (b) The image acquired in June 2009.

B. EVALUATION CRITERIA AND PARAMETER SETTINGS

To analysis the change detection results quantitatively, here we give a brief introduction of the evaluation criteria. In SAR image change detection for two classes, we compare the reference map with the one generated by a certain approach to get the number of pixels belonging to unchanged areas but wrongly detected as changed pixels and of pixels belonging to changed areas but undetected. We call the two numbers FA (false alarms) and MA (missed alarms) for short respectively. And in SAR image change detection for three classes, FA and MA can be further refined by distinguishing the positive and negative changes. Therefore, positive missed alarms (PMA), negative missed alarms (NMA), positive false alarms (PFA), and negative false alarms (NFA) are defined as follows.

Positive Missed alarms: The number of positive changed pixels in the reference map that are undetected when compared to the change detection result.

Negative Missed alarms: The number of negative changed pixels in the reference map that are undetected when compared to the change detection result.

Positive False alarms: The number of positive changed pixels in the change detection result that are incorrectly classified when compared to the reference map.

Negative False alarms: The number of negative changed pixels in the change detection result that are incorrectly classified when compared to the reference map.

Therefore the total errors (TE) is the summation of these alarms. To evaluate the result further, we define the

percentage correct classification (PCC) as [44]

$$PCC = \frac{N - PMA - NMA - FFA - NFA}{N}$$

and it expresses the correct rate of the result roughly. N is the number of the pixels of the difference image.

In order to assess the effectiveness of the proposed image change detection approach (written as MOLIGA), we consider the above data sets and compare the results provided by the proposed technique with those obtained by four methods which are widely used in change detection task. The generalized Gaussian KI (GGKI) thresholding [14], [18] which select one or two global threshold automatically is a representative threshold algorithm and successfully used in SAR image change detection. Moreover, the fuzzy C-means algorithm (FCM) (serving as a fundamental one) and the fuzzy local information C-mean algorithm (FLICM) [20] are used to compare with the proposed algorithm. Furthermore, a multi-objective genetic clustering (MOGA) proposed in [27] is chosen as a method used to compare with the proposed technique. MOGA and the proposed algorithm are executed for 100 generations with fixed population size 100. The crossover and mutation probabilities are fixed as 0.8 and 0.01. The best choice for the fuzzy exponent m in FCM, FLICM, MOGA, and MOLIGA is probably in the interval [1.5,2/5]. In most cases, we set $m = 2$. The window size used in FLICM and MOLIGA is not the same in different experiments. If SAR images have much speckle noise, the window size should be large. In the experiments of Yellow River data sets, the window size is 5×5. And for the other data sets, the window size is 3×3. In the experiments, the algorithms are carried out independently for thirty times. And the values of the criteria are the average values.

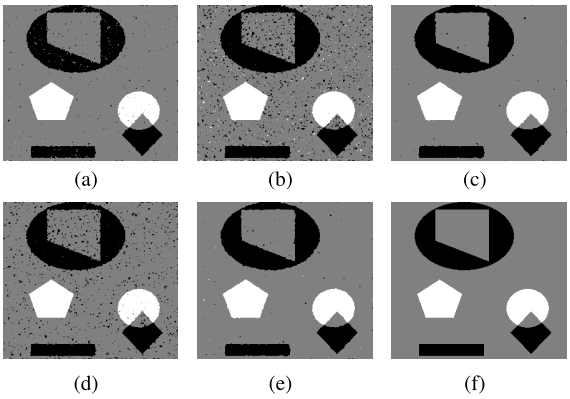

FIGURE 8. Change detection maps of the simulated data set I at ENL = 5 with the mean-ratio operator obtained by (a) GGKI, (b) FCM, (c) FLICM, (d) MOGA, and (e) MOLIGA (proposed method). (f) is the reference map.

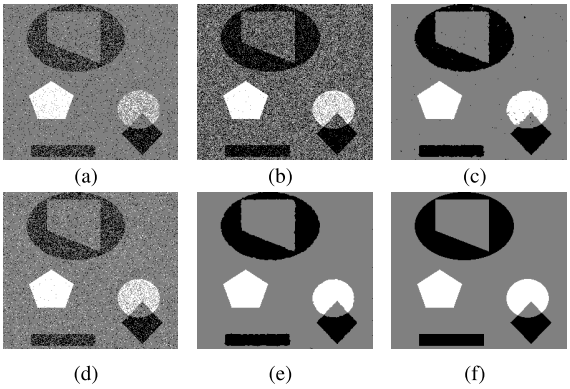

FIGURE 9. Change detection maps of the simulated data set I at ENL = 5 with the log-ratio operator obtained by (a) GGKI, (b) FCM, (c) FLICM, (d) MOGA, and (e) MOLIGA (proposed method). (f) is the reference map.

V. EXPERIMENTAL RESULTS

In this section, the change detection results obtained by five representative method are given. The results of the experiments are shown in two ways: one is to exhibit the final maps obtained by the five algorithms, and the other is to provide some values of criteria to evaluate the final maps.

A. RESULTS ON THE SIMULATED DATA SET I

Fig. 8 shows the change detection results of the simulated data set I at ENL = 5 by classifying the SAR mean-ratio image into three classes using five different algorithms. Obviously, the results obtained by GGKI, FLICM, and MOLIGA are better than those by FCM and MOGA. FLICM and MOLIGA are robust to noise by incorporating the local information. The change detection map obtained by MOGA has less noise than that by FCM. MOGA provides a set of change detection results and the user can choose suitable one from them according to problem requirements. Similarly, MOLIGA has a better result than FLICM because MOLIGA optimizes three objectives simultaneously and works well on various data sets. Change maps of the simulated data set I at ENL = 5 with log-ratio operator obtained by five algorithms are shown in Fig. 9. The change detection maps obtained by GGKI, FCM, and MOGA have much noise. However, the background of the change detection maps obtained by FLICM and MOLIGA is clear.

The results of the simulated data set I at ENL = 5 are shown in Table 1. The GGKI method has the largest NMAs and the FCM algorithm has the largest PFAs. The FCM algorithms as a fundamental method has the worst results. The FLICM algorithm has a better performance by incorporating local spatial and gray level information into the FCM algorithm. From Table 1 and Fig. 10, the proposed algorithm has the smallest TEs and the largest PCCs which combines the respective advantages of the FLICM algorithm and the MOGA method. We exhibit the values of PCCs at different ENL values in the form of broken line graph shown in Fig. 11. When noise level is low, the distinction of the performance of these algorithms shown in Fig. 11(a) is small. However, PCCs obtained by GGKI, FCM, and MOGA are much smaller than others sown in Fig. 11(b). the proposed algorithm has the best results both in Fig. 11(a) and (b) at different ENLs, i.e. it works well both in classifying the SAR mean-ratio and log-ratio images.

TABLE 1. Comparison of the change detection results of the simulated data set I at ENL = 5 with five different methods for SAR Mean-ratio and Log-ratio images.

Ratio	Method	PMA	NMA	PFA	NFA	TE	PCC(%)
MR	GGKI	61	477	26	356	920	98.7
	FCM	10	74	395	2957	3436	95.15
	FLICM	26	90	69	372	557	99.21
	MOGA	65	95	22	2283	2465	96.52
	MOLIGA	16	143	105	282	546	99.23
LR	GGKI	1721	5250	498	2106	9575	86.47
	FCM	819	1446	2163	13438	17866	74.76
	FLICM	213	260	24	247	744	98.95
	MOGA	819	4937	2163	2428	10347	85.38
	MOLIGA	124	216	5	136	481	99.32

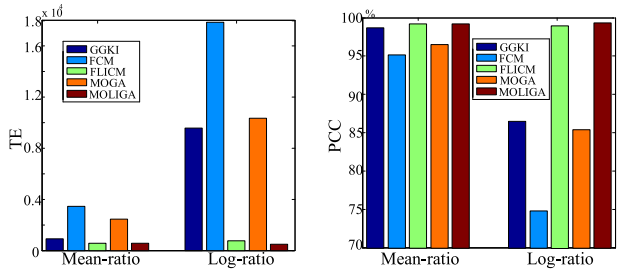

FIGURE 10. Comparison of results obtained by different methods according to the values of TE and PCC of the simulated data set I. (a) shows the average values of TE. (b) shows the average values of PCC.

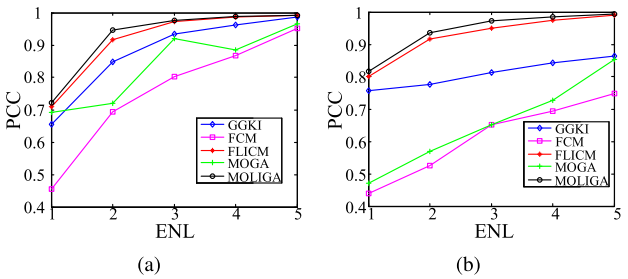

FIGURE 11. The values of PCC of the simulated data set I obtained by five methods at different ENLs for (a) mean-ratio image and (b) log-ratio image.

B. RESULTS ON THE SIMULATED DATA SET II

The experiment on the simulated data set II is exhibited as well as the previous experiment. The results of the simulated data set II at ENL = 5 obtained by five algorithms are shown in Fig. 12 and Fig. 13. As shown in Fig. 12, the change detection map obtained by the proposed algorithm has less noise than those obtained by the other four algorithms. From intuitive vision of Fig. 13, the change detection result in the upper left corner in (a) is bad compared with the reference image shown in (f). The FCM algorithm and the MOGA method are sensitive to noise. The FLICM algorithm and the proposed method obtain better results than others.

Table 2 shows the results of the simulated data set II at ENL = 5. The FCM algorithm has the larggest NFAs and therefore, the PCCs of this method are lowest to 88.11% and 68.5%. The proposed approach obtains the smallest

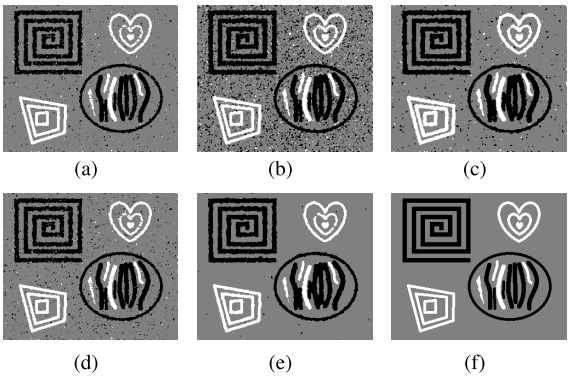

FIGURE 12. Change detection maps of the simulated data set II at ENL = 5 with the mean-ratio operator obtained by (a) GGKI, (b) FCM, (c) FLICM, (d) MOGA, and (e) MOLIGA (proposed method). (f) is the reference map.

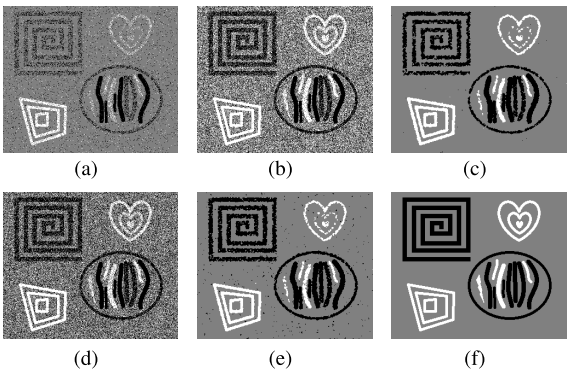

FIGURE 13. Change detection maps of the simulated data set II at ENL = 5 with the log-ratio operator obtained by (a) GGKI, (b) FCM, (c) FLICM, (d) MOGA, and (e) MOLIGA (proposed method). (f) is the reference map.

TABLE 2. Comparison of the change detection results of the simulated data set II at ENL = 5 with five different methods for SAR Mean-ratio and Log-ratio images.

Ratio	Method	PMA	NMA	PFA	NFA	TE	PCC(%)
MR	GGKI	534	1346	430	1349	3659	95.76
	FCM	243	248	1691	8086	10268	88.11
	FLICM	108	271	1447	2822	4648	94.62
	MOGA	454	914	561	2276	4205	95.13
	MOLIGA	322	275	387	1384	2368	97.26
LR	GGKI	2946	7740	985	2335	14006	83.78
	FCM	658	3659	12687	10197	27201	68.5
	FLICM	1151	2876	246	559	4832	94.4
	MOGA	1113	2988	7211	13108	24420	71.72
	MOLIGA	1192	1493	202	1267	4154	95.19

TEs (2368 and 4154) and largest PCCs (97.26% and 95.19%). From Fig. 15, the curves in (b) is more stationary than those in (a). For SAR mean-ratio images at ENL = 5, all these methods obtain good results. The proposed algorithm has the largest PCCs in classifying both SAR mean-ratio and log-ratio images at different ENLs. To sum up, the proposed approach fits the situation where the changed areas have complicated textures.

C. RESULTS ON THE SAN FRANCISCO DATA SET

The results of the experiment on the San Francisco data set are shown in Fig. 16 and Fig. 17. As shown

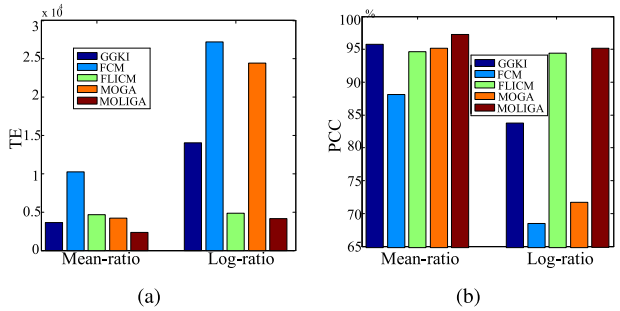

FIGURE 14. Comparison of results obtained by different methods according to the values of TE and PCC of the simulated data set II. (a) shows the average values of TE. (b) shows the average values of PCC.

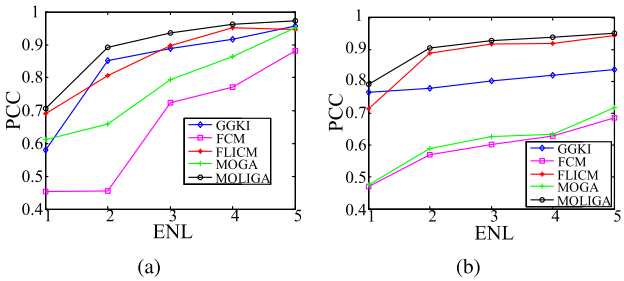

FIGURE 15. The values of PCC of the simulated data set II obtained by five methods at different ENLs for (a) mean-ratio image and (b) log-ratio image.

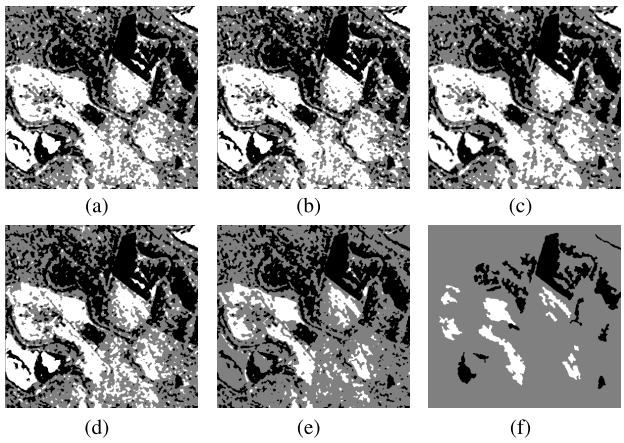

FIGURE 16. Change detection maps of the San Francisco data set with the mean-ratio operator obtained by (a) GGKI, (b) FCM, (c) FLICM, (d) MOGA, and (e) MOLIGA (proposed method). (f) is the reference map.

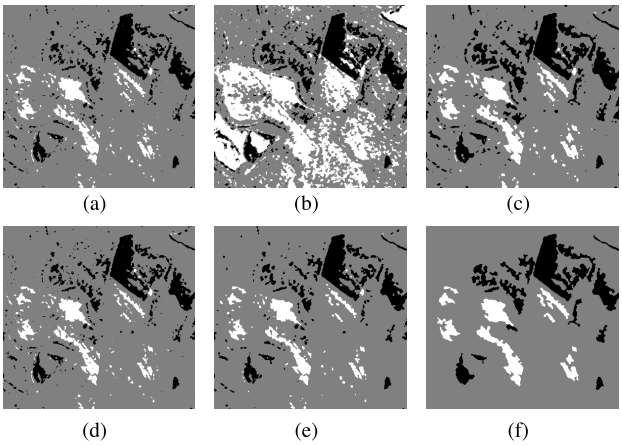

FIGURE 17. Change detection maps of the San Francisco data set with the log-ratio operator obtained by (a) GGKI, (b) FCM, (c) FLICM, (d) MOGA, and (e) MOLIGA (proposed method). (f) is the reference map.

TABLE 3. Comparison of the change detection results of the san francisco data set with five different methods for SAR Mean-ratio and Log-ratio images.

Ratio	Method	PMA	NMA	PFA	NFA	TE	PCC(%)
MR	GGKI	51	54	32991	28304	61400	57.45
	FCM	36	42	36036	31941	68055	52.84
	FLICM	37	39	32666	28297	61039	57.7
	MOGA	69	42	24311	31941	56363	60.94
	MOLIGA	150	54	7515	28307	36026	75.03
LR	GGKI	1641	3400	1368	1932	8341	94.22
	FCM	68	1960	30024	3990	36042	75.02
	FLICM	553	662	2121	4565	7901	94.52
	MOGA	1908	3275	1123	2084	8390	94.19
	MOLIGA	1756	3074	758	1399	6987	95.16

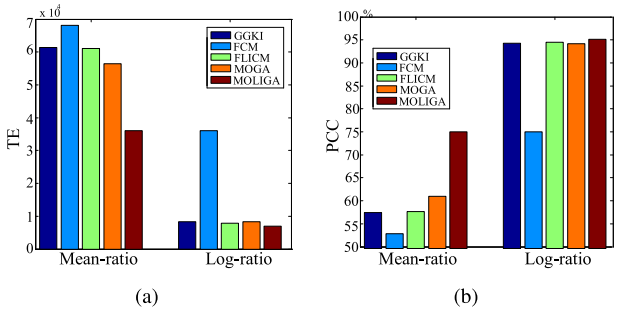

FIGURE 18. Comparison of results obtained by different methods according to the values of TE and PCC of the San Francisco data set I. (a) shows the average values of TE. (b) shows the average values of PCC.

in Fig. 16, many unchanged areas are incorrectly classified into changed classes compared with the reference image shown in Fig. 16(f). And in Fig. 17, these methods except the FCM algorithm have obtained satisfactory results. FLICM and the proposed algorithm have better results than others as they incorporate local information which makes a contribution to reducing the corruption of speckle noise.

As shown in Table 3, for change detection in SAR log-ratio image, the values of TE and PCC of the proposed method are a little less than those of FLICM. However, for change detection in SAR mean-ratio image, the proposed method are much better than FLICM. Furthermore, the MOGA method obtains a better results than FCM, FLICM, and GGKI because a number of fuzzy cluster validity indexes are optimized to get a more suitable partitioning. As shown in Fig. 18, the proposed algorithm obtains the smallest TEs and the largest PCCs, which indicates the effectiveness of the proposed technique.

D. RESULTS ON THE YELLOW RIVER DATA SET I

Fig. 19 and Fig. 20 present a visual comparison between the change detection maps obtained by five different algorithms. As shown in Fig. 19, all these algorithm obtain abundant changed areas compared with the ground truth image shown

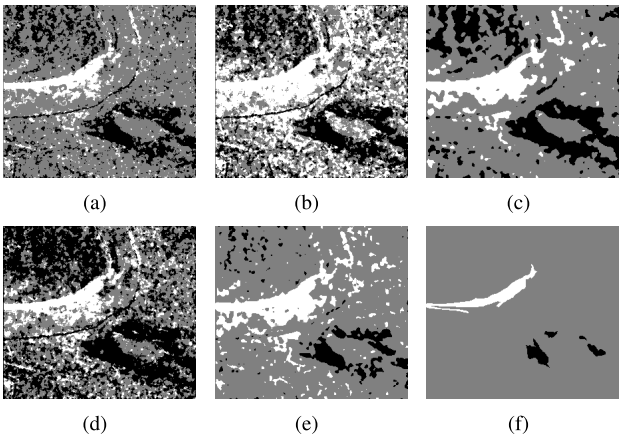

FIGURE 19. Change detection maps of the Yellow River data set I with the mean-ratio operator obtained by (a) GGKI, (b) FCM, (c) FLICM, (d) MOGA, and (e) MOLIGA (proposed method). (f) is the reference map.

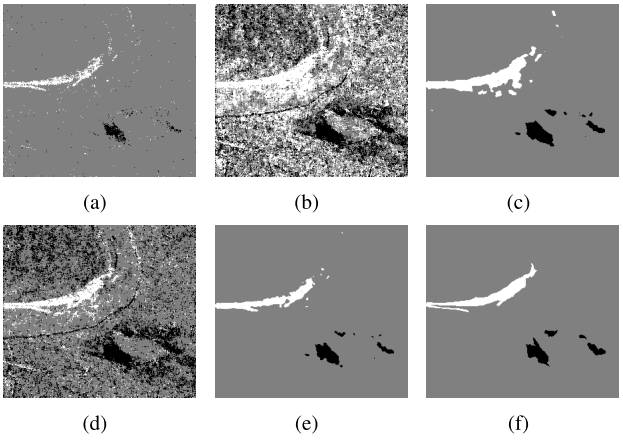

FIGURE 20. Change detection maps of the Yellow River data set I with the log-ratio operator obtained by (a) GGKI, (b) FCM, (c) FLICM, (d) MOGA, and (e) MOLIGA (proposed method). (f) is the reference map.

in Fig. 19(f). In the process of generating SAR mean-ratio images, mean filter is used to smooth speckle noise present in SAR images. In the mean scale, many pixels are classified into changed areas. However, the proposed algorithm still have a better result than others. As shown in Fig. 20, by incorporating local information into the FCM algorithm, the change detection results of the FLICM algorithm and the proposed algorithm are closer to the ground truth image.

From Table 4, for change detection in SAR mean-ratio image, the proposed algorithm has the smallest NFAs (4129) and NFAs of the other algorithm are larger than 10000. Therefore the proposed algorithm has the highest PCC which verifies the effectiveness of the proposed method. As shown in Fig. 21, for change detection in SAR log-ratio image, the FLICM algorithm and the proposed method have almost the same TEs and PCCs.

E. RESULTS ON THE YELLOW RIVER DATA SET II

The Yellow River Data Set II is more complicated than the previous data sets. It is difficult to identify the positive and negative changed areas clearly. This data set has greater

TABLE 4. Comparison of the change detection results of the yellow river data set I with five different methods for SAR Mean-ratio and Log-ratio images.

Ratio	Method	PMA	NMA	PFA	NFA	TE	PCC(%)
MR	GGKI	128	23	5067	13528	18746	75.14
	FCM	22	19	22769	17014	39824	47.18
	FLICM	35	4	6733	14302	21074	72.05
	MOGA	78	12	8703	30458	39251	47.94
	MOLIGA	29	22	8528	4129	12708	83.15
LR	GGKI	945	610	421	157	2133	97.17
	FCM	123	60	21023	13113	34319	54.48
	FLICM	147	145	1276	347	1915	97.46
	MOGA	377	48	3540	15759	19724	73.84
	MOLIGA	588	271	332	139	1330	98.24

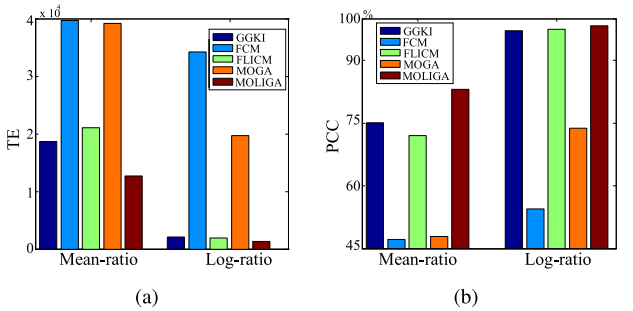

FIGURE 21. Comparison of results obtained by different methods according to the values of TE and PCC of the Yellow River data set I. (a) shows the average values of TE. (b) shows the average values of PCC.

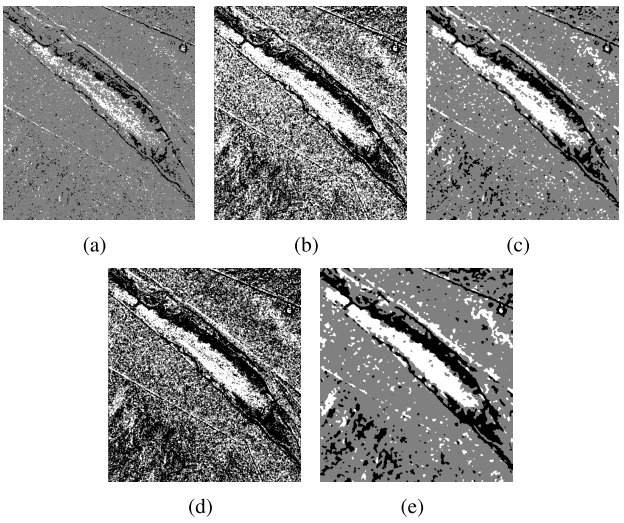

FIGURE 22. Change detection maps of the Yellow River data set II with the mean-ratio operator obtained by (a) GGKI, (b) FCM, (c) FLICM, (d) MOGA, and (e) MOLIGA (proposed method).

speckle noise, which is hard to obtain good change detection results. For the Yellow River Data Set II, there is no ground truth image provided to quantitative measure. Hence, a visual analysis is used to compare the change detection results obtained by five algorithms. Fig. 22 shows the final maps obtained by five algorithms using SAR mean-ratio image and Fig. 23 presents the change detection maps with log-ratio operator. The change detection maps obtained by FCM and MOGA are sensitive to noise, which have many spots shown in Fig. 22(b), Fig. 22(d), Fig. 23(b), and Fig. 23(d). The changed areas obtained by the proposed algorithm shown in Fig. 23(e) is more clear than others.

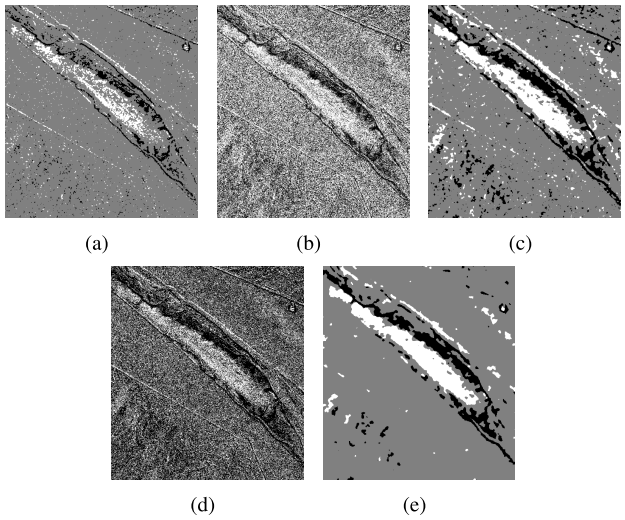

FIGURE 23. Change detection maps of the Yellow River data set II with the log-ratio operator obtained by (a) GGKI, (b) FCM, (c) FLICM, (d) MOGA, and (e) MOLIGA (proposed method).

VI. CONCLUDING REMARKS

In this paper, in order to detect the positive and negative changes in multitemporal SAR images, change detection in SAR images is reformulated as a three-class classification problem. And the widely used mean-ratio and log-ratio operators are extended to generate three-class SAR ratio images. In order to classify the SAR ratio images into three classes, we have presented a multi-objective clustering approach for three-class SAR image change detection. The proposed method is robust to speckle noise present in SAR images by expoliting local spatial and gray level information. Due to the incorporation of local information, the computational complexity of the proposed method becomes quite high. However, experiments on two simulated and three real SAR data sets have shown the advantage of the proposed method. In the future, we will explore more objective functions to be suitable for SAR image change detection and pay interest in optimizing the search strategy to reduce the time complexity.

REFERENCES

[1] Y. Lei, X. Liu, J. Shi, C. Lei, and J. Wang, "Multiscale superpixel segmentation with deep features for change detection," *IEEE Access*, vol. 7, pp. 36600–36616, 2019.
[2] Z. Lv, T. Liu, J. A. Benediktsson, and H. Du, "Novel land cover change detection method based on K-means clustering and adaptive majority voting using bitemporal remote sensing images," *IEEE Access*, vol. 7, pp. 34425–34437, 2019.
[3] Y. Zhong, W. Liu, J. Zhao, and L. Zhang, "Change detection based on pulse-coupled neural networks and the NMI feature for high spatial resolution remote sensing imagery," *IEEE Geosci. Remote Sens. Lett.*, vol. 12, no. 3, pp. 537–541, Mar. 2015.
[4] L. Ma, Z. Jia, Y. Yu, J. Yang, and N. K. Kasabov, "Multi-spectral image change detection based on band selection and single-band iterative weighting," *IEEE Access*, vol. 7, pp. 27948–27956, 2019.
[5] S. A. Azzouzi, A. Vidal-Pantaleoni, and H. A. Bentounes, "Desertification monitoring in Biskra, algeria, with Landsat imagery by means of supervised classification and change detection methods," *IEEE Access*, vol. 5, pp. 9065–9072, 2017.
[6] P. Sinha and L. Kumar, "Independent two-step thresholding of binary images in inter-annual land cover change/no-change identification," *ISPRS J. Photogramm. Remote Sens.*, vol. 81, pp. 31–43, Jul. 2013.
[7] H. Dong, W. Ma, Y. Wu, M. Gong, and L. Jiao, "Local descriptor learning for change detection in synthetic aperture radar images via convolutional neural networks," *IEEE Access*, vol. 7, pp. 15389–15403, 2019.
[8] L. Liu, Z. Jia, J. Yang, and N. K. Kasabov, "SAR image change detection based on mathematical morphology and the K-means clustering algorithm," *IEEE Access*, vol. 7, pp. 43970–43978, 2019.
[9] O. Yousif and Y. Ban, "Improving urban change detection from multitemporal SAR images using PCA-NLM," *IEEE Trans. Geosci. Remote Sens.*, vol. 51, no. 4, pp. 2032–2041, Apr. 2013.
[10] J. Inglada and G. Mercier, "A new statistical similarity measure for change detection in multitemporal SAR images and its extension to multiscale change analysis," *IEEE Trans. Geosci. Remote Sens.*, vol. 45, no. 5, pp. 1432–1445, May 2007.
[11] M. Gong, Y. Li, L. Jiao, M. Jia, and L. Su, "SAR change detection based on intensity and texture changes," *ISPRS J. Photogramm. Remote Sens.*, vol. 93, pp. 123–135, Jul. 2014.
[12] O. Yousif and Y. Ban, "Improving SAR-based urban change detection by combining MAP-MRF classifier and nonlocal means similarity weights," *IEEE J. Sel. Topics Appl. Earth Observ. Remote Sens.*, vol. 7, no. 10, pp. 4288–4300, Oct. 2014.
[13] F. Bujor, E. Trouvé, L. Valet, J.-M. Nicolas, and J.-P. Rudant, "Application of log-cumulants to the detection of spatiotemporal discontinuities in multitemporal SAR images," *IEEE Trans. Geosci. Remote Sens.*, vol. 42, no. 10, pp. 2073–2084, Oct. 2004.
[14] Y. Bazi, L. Bruzzone, and F. Melgani, "An unsupervised approach based on the generalized Gaussian model to automatic change detection in multitemporal SAR images," *IEEE Trans. Geosci. Remote Sens.*, vol. 43, no. 4, pp. 874–887, Apr. 2005.
[15] Y. Ban and O. A. Yousif, "Multitemporal spaceborne SAR data for urban change detection in China," *IEEE J. Sel. Topics Appl. Earth Observat. Remote Sens.*, vol. 5, no. 4, pp. 1087–1094, Aug. 2012.
[16] H. Hu and Y. Ban, "Unsupervised change detection in multitemporal SAR images over large urban areas," *IEEE J. Sel. Topics Appl. Earth Observ. Remote Sens.*, vol. 7, no. 8, pp. 3248–3261, Aug. 2014.
[17] M. Gong, L. Su, M. Jia, and W. Chen, "Fuzzy clustering with a modified MRF energy function for change detection in synthetic aperture radar images," *IEEE Trans. Fuzzy Syst.*, vol. 22, no. 1, pp. 98–109, Feb. 2014.
[18] Y. Bazi, L. Bruzzone, and F. Melgani, "Automatic identification of the number and values of decision thresholds in the log-ratio image for change detection in SAR images," *IEEE Geosci. Remote Sens. Lett.*, vol. 3, no. 3, pp. 349–353, Jul. 2006.
[19] H. Xie, L. E. Pierce, and F. T. Ulaby, "SAR speckle reduction using wavelet denoising and Markov random field modeling," *IEEE Trans. Geosci. Remote Sens.*, vol. 40, no. 10, pp. 2196–2212, Oct. 2002.
[20] S. Krinidis and V. Chatzis, "A robust fuzzy local information C-means clustering algorithm," *IEEE Trans. Image Process.*, vol. 19, no. 5, pp. 1328–1337, May 2010.
[21] M. Gong, Z. Zhou, and J. Ma, "Change detection in synthetic aperture radar images based on image fusion and fuzzy clustering," *IEEE Trans. Image Process.*, vol. 21, no. 4, pp. 2141–2151, Apr. 2012.
[22] C. C. Coello, G. B. Lamont, and D. A. van Veldhuizen, *Evolutionary Algorithms for Solving Multi-Objective Problems*. Norwell, MA, USA: Kluwer, 2002.
[23] C. M. Fonseca and P. J. Fleming, "An overview of evolutionary algorithms in multiobjective optimization," *Evol. Comput.*, vol. 3, no. 1, pp. 1–16, 1995.
[24] A. Mukhopadhyay, U. Maulik, S. Bandyopadhyay, and C. A. C. Coello, "Survey of multiobjective evolutionary algorithms for data mining: Part II," *IEEE Trans. Evol. Comput.*, vol. 18, no. 1, pp. 20–35, Feb. 2014.
[25] A. Mukhopadhyay and U. Maulik, "A multiobjective approach to MR brain image segmentation," *Appl. Soft Comput.*, vol. 11, no. 1, pp. 872–880, Jan. 2011.
[26] A. Mukhopadhyay, U. Maulik, and S. Bandyopadhyay, "Multiobjective genetic clustering with ensemble among Pareto front solutions: Application to MRI brain image segmentation," in *Proc. 7th Int. Conf. Adv. Pattern Recognit.*, Feb. 2009, pp. 236–239.
[27] S. Bandyopadhyay, U. Maulik, and A. Mukhopadhyay, "Multiobjective genetic clustering for pixel classification in remote sensing imagery," *IEEE Trans. Geosci. Remote Sens.*, vol. 45, no. 5, pp. 1506–1511, May 2007.
[28] A. Mukhopadhyay and U. Maulik, "Unsupervised pixel classification in satellite imagery using multiobjective fuzzy clustering combined with SVM classifier," *IEEE Trans. Geosci. Remote Sens.*, vol. 47, no. 4, pp. 1132–1138, Apr. 2009.

[29] J. Handl and J. Knowles, "An evolutionary approach to multiobjective clustering," *IEEE Trans. Evol. Comput.*, vol. 11, no. 1, pp. 56–76, Feb. 2007.
[30] X. L. Xie and G. Beni, "A validity measure for fuzzy clustering," *IEEE Trans. Pattern Anal. Mach. Intell.*, vol. 13, no. 8, pp. 841–847, Aug. 1991.
[31] J. C. Bezdek, *Pattern Recognition With Fuzzy Objective Function Algorithms*. New York, NY, USA: Plenum, 1981.
[32] D. W. Corne, N. R. Jerram, J. D. Knowles, and M. J. Oates, "PESA-II: Region-based selection in evolutionary multiobjective optimization," in *Proc. 3rd Annu. Conf. Genetic Evol. Comput.*, 2001, pp. 283–290.
[33] K. Deb, A. Pratap, S. Agarwal, and T. Meyarivan, "A fast and elitist multiobjective genetic algorithm: NSGA-II," *IEEE Trans. Evol. Comput.*, vol. 6, no. 2, pp. 182–197, Apr. 2002.
[34] A. Mukhopadhyay, U. Maulik, and S. Bandyopadhyay, "Multiobjective genetic algorithm-based fuzzy clustering of categorical attributes," *IEEE Trans. Evol. Comput.*, vol. 13, no. 5, pp. 991–1005, Oct. 2009.
[35] K. Deb, *Multi-Objective Optimization Using Evolutionary Algorithms*. New York, NY, USA: Wiley, 2001.
[36] K. Miettinen, *Nonlinear Multiobjective Optimization*. Norwell, MA, USA: Kluwer, 1999.
[37] J. D. Schaffer, "Multiple objective optimization with vector evaluated genetic algorithms," in *Proc. 1st Int. Conf. Genetic Algorithms Appl.*, 1985, pp. 93–100.
[38] C. A. C. Coello, G. T. Pulido, and M. S. Lechuga, "Handling multiple objectives with particle swarm optimization," *IEEE Trans. Evol. Comput.*, vol. 8, no. 3, pp. 256–279, Jun. 2004.
[39] J. Knowles and D. Corne, "The Pareto archived evolution strategy: A new baseline algorithm for Pareto multiobjective optimisation," in *Proc. Congr. Evol. Comput.*, 1999, pp. 98–105.
[40] E. Zitzler, M. Laumanns, and L. Thiele, "SPEA2: Improving the strength Pareto evolutionary algorithm," in *Proc. Evol. Methods Design Optim. Control Appl. Ind. Problems*, 2002, pp. 95–100.
[41] Q. Zhang and H. Li, "MOEA/D: A multiobjective evolutionary algorithm based on decomposition," *IEEE Trans. Evol. Comput.*, vol. 11, no. 6, pp. 712–731, Dec. 2007.
[42] R. J. Dekker, "Speckle filtering in satellite SAR change detection imagery," *Int. J. Remote Sens.*, vol. 19, no. 6, pp. 1133–1146, 1998.
[43] K. Deb, S. Agrawal, A. Pratap, and T. Meyarivan, "A fast elitist non-dominated sorting genetic algorithm for multi-objective optimization: NSGA-II," in *Proc. Int. Conf. Parallel Problem Solving Nature*, 2000, pp. 849–858.
[44] P. L. Rosin and E. Ioannidis, "Evaluation of global image thresholding for change detection," *Pattern Recognit. Lett.*, vol. 24, no. 14, pp. 2345–2356, 2003.

SHUANG LIANG received the B.S. degree in electronic information engineering from Xidian University, Xi'an, China, in 2012, where he is currently pursuing the Ph.D. degree in pattern recognition and intelligent systems with the Key Laboratory of Intelligent Perception and Image Understanding, Ministry of Education.

His research interests include computational intelligence, multi-objective optimization, and distributed computing.

HAO LI received the B.S. degree in electronic engineering and the Ph.D. degree in pattern recognition and intelligent systems from Xidian University, Xi'an, China, in 2013 and 2018, respectively, where he is currently a Lecturer with the School of Electronic Engineering.

His research interests include computational intelligence and machine learning.

YUN ZHU received the B.S. degree in electronic information engineering and the Ph.D. degree in signal and information processing from Xidian University, Xi'an, China, in 2012 and 2019, respectively.

She is currently a Lecturer with the School of Computer Science, Shaanxi Normal University. Her research interests include the multi-objective optimization, multi-sensor multi-target information fusion, filtering theory, and radar signal processing.

MAOGUO GONG (M'07–SM'14) received the B.S. degree (Hons.) in electronic engineering and the Ph.D. degree in electronic science and technology from Xidian University, Xi'an, China, in 2003 and 2009, respectively.

Since 2006, he has been a Teacher with Xidian University. In 2008 and 2010, he was promoted as an Associate Professor and a Full Professor, respectively, with exceptive admission. His research interests include computational intelligence with applications to optimization, learning, data mining, and image understanding.

Dr. Gong is an Executive Committee Member of the Chinese Association for Artificial Intelligence and a Senior Member of the Chinese Computer Federation. He received the prestigious National Program for the support of Top-Notch Young Professionals from the Central Organization Department of China, the Excellent Young Scientist Foundation from the National Natural Science Foundation of China, and the New Century Excellent Talent in University from the Ministry of Education of China. He is the Vice Chair of the IEEE Computational Intelligence Society Task Force on Memetic Computing. He is also the Associate Editor of the IEEE TRANSACTIONS ON EVOLUTIONARY COMPUTATION and the IEEE TRANSATIONS ON NEURAL NETWORKS AND LEARNING SYSTEMS.